Effect of microstructure on tensile properties of quenched and partitioned martensitic stainless steels

Sierra-Soraluce, A.; Li, G.; Santofimia, M. J.; Molina-Aldareguia, J. M.; Smith, A.; Muratori, M.; Sabirov, I.

DOI
10.1016/j.msea.2022.144540

Publication date
2023

Document Version
Final published version

Published in
Materials Science and Engineering A

Materials Science & Engineering A 864 (2023) 144540

Contents lists available at ScienceDirect

Materials Science & Engineering A

journal homepage: www.elsevier.com/locate/msea

Effect of microstructure on tensile properties of quenched and partitioned martensitic stainless steels

A. Sierra-Soraluce [a,*], G. Li [b], M.J. Santofimia [b], J.M. Molina-Aldareguia [c,a], A. Smith [d], M. Muratori [e], I. Sabirov [a]

[a] IMDEA Materials Institute, Eric Kandel, 2, Getafe, 28906, Spain
[b] Department of Materials Science and Engineering, Delft University of Technology, Mekelweg 2, CD Delft, 2628, the Netherlands
[c] Department of Mechanical Engineering, Universidad Politécnica de Madrid, José Gutierréz Abascal, 2, Madrid, 28006, Spain
[d] RINA Consulting - Centro Sviluppo Materiali SpA, Castel Romano 100, Rome, 00128, Italy
[e] Acerinox Europa S.A.U., Acerinox Europa, Los Barrios, 11379, Spain

ARTICLE INFO

Keywords:
Stainless steel
Quenching and partitioning
Retained austenite
Electron backscatter diffraction
Tensile properties
Phase transformation

ABSTRACT

Quenching and partitioning (Q&P) treatment has been proven effective in manufacturing advanced high strength steels with high content of retained austenite, showing the improved balance of high strength and sufficient ductility. This method has been very well elaborated for carbon steel processing over the last two decades. Though it can also be potentially applied for processing other steel families, this has been scarcely studied. This article focuses on the effect of chemistry and heat treatment parameters on the microstructure and properties of Q&P treated martensitic stainless steels. Three different martensitic stainless steels with different contents of alloying elements are subjected to Q&P processing with varying quenching temperature or partitioning temperature and partitioning time. The tensile behavior of the Q&P treated steels is studied. The effect of chemistry and Q&P treatment parameters on the microstructure and tensile properties is analyzed. The effect of plastic deformation on the microstructure of the Q&P treated steels is also investigated. It is demonstrated that the Q&P treated martensitic stainless steels can show a good combination of enhanced strength and sufficient tensile ductility. Their uniform elongation increases with the increasing volume fraction of retained austenite due to the transformation induced plasticity (TRIP) effect. The ability of the martensitic matrix to accumulate plastic deformation also plays an important role. The Q&P process - microstructure - property relationship is discussed.

1. Introduction

The modern steel industry faces various challenges and risks. With a share of 17% in the energy consumption of the industrial sector, steel belongs to the engineering sector with the highest relevance concerning reduction measures for energy consumption. The world's ambitions to mitigate global warming affect the steel industry, as it accounts for about 20% of the carbon emissions of manufacturing industries [1]. Two approaches can address these challenges: developing new materials and manufacturing processes or optimizing existing ones. Developing a new material and process is not always required, as the optimization of the existing materials can lead to the same successful outcome at a lower cost. By modifying manufacturing parameters and heat treatments, it is possible to increase the energy efficiency of the manufacturing process and enhance the mechanical performance of already-existing materials [2]. The latter can be utilized for manufacturing more energy-efficient and less contaminant components. For example, thinner elements of automotive body-in-white parts made of advanced high strength steel (AHSS) reduce their weight resulting in less gasoline use and lower carbon emissions [3].

The "quenching and partitioning" (Q&P) heat treatment was first proposed in 2003 as a novel tool for the microstructural design in carbon steels [4]. This process is based on quenching austenite to an intermediate temperature between the martensite start (M_s) and martensite finish (M_f) followed by a partitioning treatment at quenching temperature or above to enrich the remaining austenite with carbon, thereby stabilizing it to room temperature (Fig. 1). The presence of retained austenite in the final microstructure enables the transformation induced plasticity (TRIP) effect, which increases the strain hardening ability and ductility due to the austenite → martensite transformation during plastic

* Corresponding author.
E-mail address: andres.sierra@imdea.org (A. Sierra-Soraluce).

https://doi.org/10.1016/j.msea.2022.144540
Received 25 October 2022; Received in revised form 21 December 2022; Accepted 22 December 2022
Available online 26 December 2022

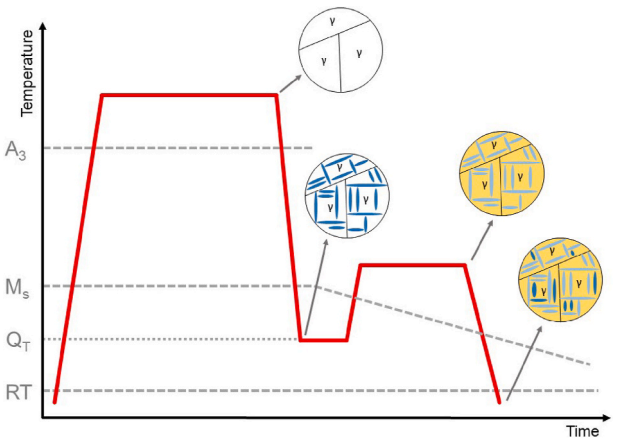

Fig. 1. A schematic presentation of the Q&P heat treatment, where A_3 indicates the temperature above which only austenite is present in the microstructure, M_S martensite start temperature, QT quenching temperature and RT room temperature.

deformation [5]. Hence, a better balance of high strength and sufficient ductility is obtained compared with a typical quenching and tempering heat treatment [6–9].

The steels processed using this heat treatment have been referred to as "Q&P steels". They belong to the third generation of AHSS. The chemical composition of the Q&P steels is designed to enable the stabilization of austenite via carbon partitioning. Alloying elements that prevent carbide precipitation, such as silicon, are expressly introduced to facilitate the partitioning process. Thus, the alloying requirements for this heat treatment are quite lenient, making this heat treatment potentially applicable to a wide range of alloys.

Carbon steels have been thoroughly investigated as Q&P steels, proven by the extensive bibliography [6–9]. The main outcomes of these studies can be roughly summarized as follows. The ultimate tensile strength of the Q&P treated carbon steels reported in the literature was from ~1000 MPa to ~2000 MPa, with total elongation ranging from ~5 to ~25% [6]. Both strength and ductility were strongly dependent on the microstructure, which was determined by steel chemical composition and applied Q&P parameters. The Q&P processing can lead to microstructures of tempered martensite with a high volume fraction of retained austenite [6–9]. Its content, morphology and mechanical stability play a key role in determining the mechanical behaviour and properties of Q&P steels. Mechanical stability of retained austenite is determined by various factors including carbon content, size and its crystallographic orientation [10]. Gradual austenite-martensite phase transformation is required during plastic deformation to achieve the enhanced strain hardening ability, tensile ductility and ultimate tensile strength [5]. This can be done via intelligent microstructural design by inducing austenite grains with varying transformation potential.

Meanwhile, few investigations have focused on using Q&P treatment for martensitic stainless steels. The Q&P process was successfully applied to the 410 [11,12] and 420 [13–16] martensitic stainless steels. It was shown that the volume fractions of retained austenite can reach up to 50%. The ductility of the Q&P treated AISI 410 grades was higher on average by 5% compared to their quenched and tempered counterparts [11,12]. These preliminary studies have clearly shown the potential of the Q&P treatment for processing martensitic stainless steels with improved properties. However, the research on Q&P treated martensitic stainless steels is in its infancy, and comprehensive studies are needed to understand the microstructure evolution during Q&P treatment and the alloy-process-microstructure-property relationship in these materials.

The main objective of this work was to study the effect of chemical composition and Q&P treatment parameters on the microstructure and tensile deformation behavior of three martensitic stainless steels. Special emphasis was laid on the microstructure of the deformed samples to study the role of retained austenite during plastic deformation. The obtained knowledge will enable the optimization of alloy chemistry and Q&P-process for microstructural design in martensitic stainless steels to improve their mechanical properties.

2. Materials & experimental procedures

2.1. Materials

Three martensitic stainless steels with varying chemical compositions were selected for this study. Table 1 presents the actual chemical compositions of these alloys.

The first alloy has a chemical composition similar to that of an AISI 410 grade (hereafter referred to as 410 alloy). The second alloy has increased carbon content for higher strength and austenite stabilization (hereafter referred to as 420). Slightly higher Cr contents are considered when the C content is increased to retain the steel's high corrosion resistance [14]. The third alloy has a similar composition as the second, but with increased Mn content (up to 3 wt%) and the addition of Nb and Ti as microalloying elements (hereafter referred to as 420ma). This addition of Mn leads to a notable increase in the thermal stability of the austenite to a level in which significant fractions can already be present at room temperature after quenching. As shown in the following sections, this will allow a Q&P process in which the quenching step takes place at room temperature. The addition of Ti and Nb is expected to promote the refinement of the prior austenite grains, leading to a general grain refinement in the final microstructure [17]. Finer austenite grains lead to a more efficient carbon partitioning process from martensite to austenite and facilitates carbon homogenization in the interior of the austenite grains [18].

2.2. Design of heat treatments

Two different strategies were considered in the design of heat treatments to be applied to these alloys: (i) the calculation of an optimum quenching temperature (OQT) leading to a theoretical maximum of retained austenite in the absence of competing reactions and (ii) the possibility of applying the quenching step at room temperature. The OQT can be estimated under the assumption of full carbon partitioning from martensite to austenite during the partitioning step, in the absence of reactions competing for carbon, such as carbide precipitation. Applying a Q&P process, in which the quenching temperature is equal to OQT, the martensite start temperature of the carbon-enriched austenite after partitioning is equal to room temperature. The application of quenching temperatures lower than the OQT leads to the formation of too much martensite at the quenching step, while the application of quenching temperatures higher than the OQT leads to unstable austenite after the partitioning process that would transform into fresh martensite. The mentioned condition is considered in this work to estimate the OQT corresponding to the three designed alloys.

To determine the Ms temperature, an empirical approach was used. The experimental data from literature studies on QP processing of 13 Cr martensitic stainless steels [11–16] were fitted to obtain a specific M_S equation for this type of steel. The fitting process was carried out in two steps (Fig. 2). First, an equation was applied, considering only Si and C as fitting parameters. This is shown by Eq. (1) below

$$M_S = 382.5–530.8\bullet (\%C) - 9.7\bullet (\%Si), \quad (1)$$

where the C and Si contents are considered in wt. %.

Since Eq. (1) does not take into account Mn or Cr, it was decided to refit the data again using Eq. (1), considering coefficients for Cr and Mn from the Andrews equation validated by Kung and Rayment [19] for steels with up to 12 wt % Cr and 5 wt % Mn. The result of this fit with the independent constant in Eq. (1) as the only fitting parameter gave the

Table 1
Chemical composition of the studied alloys (wt. %).

Designation	C	Mn	Si	Cr	Ni	Al	N	Nb	Ti
410	0.2	0.7	0.35	12.5	0.20	0.01	0.03	–	–
420	0.3	0.7	0.35	13.0	0.20	0.01	0.03	–	–
420ma	0.3	3.0	0.35	13.0	0.20	0.01	0.03	0.05	0.05

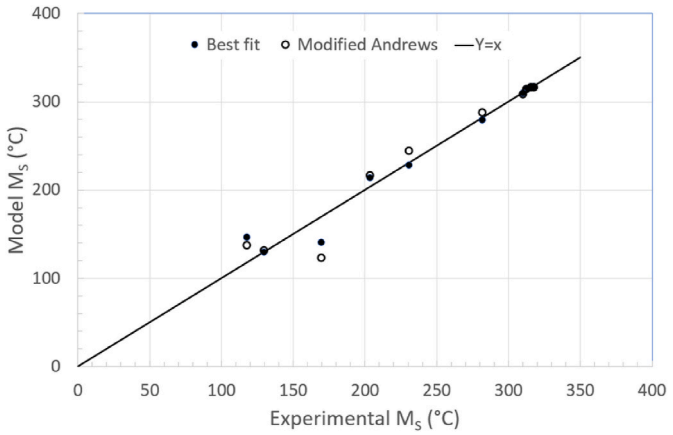

Fig. 2. Comparison of calculated values of M_S with Eq. (1) (filled symbols) and Eq. (2) (open symbols), with experimentally determined values of M_S for 13Cr steels from literature [11–16].

following equation (modified Andrews):

$$M_S = 553.7 - 530.8\bullet(\%C) - 9.7\bullet(\%Si) - 12.1\bullet(\%Cr) - 30.4\bullet(\%Mn). \quad (2)$$

By assuming M_S equal to room temperature, this equation provides the minimum carbon content that must be present in the austenite to obtain its full stabilization at room temperature. Under the conditions of full carbon partitioning from martensite to austenite, and considering austenite having the calculated carbon concentration, the carbon balance in the material is such that [20]:

$$f^{\gamma}_{OQT} \cdot (\%C)^{\gamma} = (\%C)^{alloy} \quad (3)$$

where $(\%C)^{alloy}$ is the carbon content of the alloy, and f^{γ}_{OQT} the maximum volume fraction of austenite, that can be fully stabilised at room temperature after full carbon partitioning, when the quenching temperature is equal to OQT. These theoretical maximum fractions of retained austenite are 0.30, 0.46 and 0.57 for alloys 410, 420 and 420ma, respectively. The quenching temperatures leading to these fractions of untransformed austenite are the OQT of the designed alloys.

Dilatometry experiments used to measure the M_S temperature on quenching were also considered to experimentally determine OQT based on the calculated maximum fractions of retained austenite. Fig. 3 shows the experimentally measured volume fraction of martensite as a function of undercooling below M_S on quench. These graphs demonstrate that the quenching temperatures leading to the determined theoretical maximum fractions of retained austenite are 160 °C, 122 °C and 62 °C, respectively. Although these were appropriated first estimations, in the case of alloy 420, further experiments showed that the quenching temperature of 122 °C was still leading to fresh martensite. Therefore, it was decided to reduce further the temperature considered as OQT to 99 °C.

Regarding the possibility of performing Q&P treatments with QT equal to room temperature, Fig. 3 shows that alloys 420 and 420ma still display significant fractions of retained austenite at room temperature after quenching. Particularly, volume fractions equal 17% and 35%, respectively. Therefore, in these cases, the application of room temperature quenching followed by partitioning was considered of interest. All these theoretical phase fractions will be further evaluated in experiments, as it is shown in the following sections.

In the present investigation, the partitioning condition of 450 °C for 5 min was selected to maximize carbon partitioning while minimizing the precipitation of carbides. To check this choice, the kinetic calculations were performed under constrained carbon equilibrium (CCE) and fixed interface using the model proposed by Santofimia et al. [21]. This model considers the 1 dimensional diffusion of carbon from martensite to austenite, assuming an austenite martensite film morphology, which is appropriate for the Q&P microstructures. In this case, martensite with 0.2 μm thickness was assumed to share an interface with austenite with 0.05 μm thickness. This situation corresponds to a system formed by 80% fraction martensite and 20% fraction austenite, according to Ref. [22]. Calculations were performed in half-thickness, assuming mirror conditions for different times at 450 °C. Fig. 4 shows the results of these calculations. It is seen that although the partitioning of martensite to austenite is finished in less than 1 s, the homogenization of carbon in the austenite film takes 1 s. Since the sizes of the retained austenite grains can vary in the microstructure, a partitioning time of 5 min was considered sufficient to ensure carbon homogenization in the austenite after the partitioning step.

2.3. Q&P processing

Steels were received in the form of cold-rolled sheets having a thickness of 1.5 mm. Samples having a length of 100 mm and a width of 10 mm were machined along the rolling direction. Their surface was

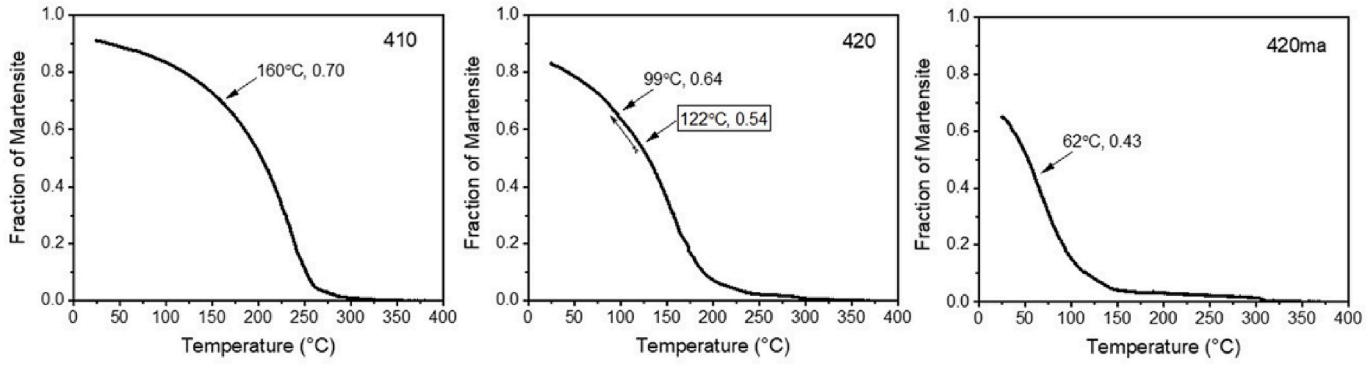

Fig. 3. Graphs showing the fraction of martensite formed during cooling as a function of temperature for alloys 410, 420 and 420ma.

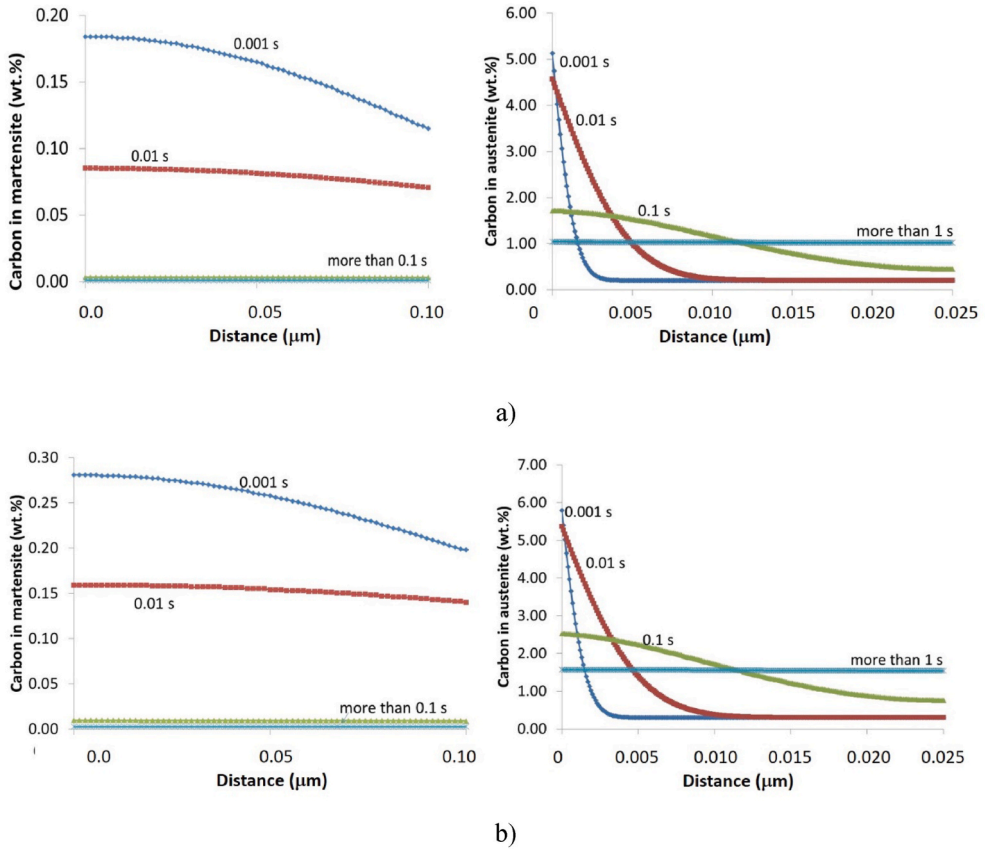

Fig. 4. Calculated carbon diffusion profiles in martensite and austenite during the partitioning step at 450 °C under CCE conditions: a) for 0.2 wt %C, b) for 0.3 wt %C.

ground, so the final thickness was 1.2 mm. These samples were Q&P treated in an argon atmosphere using a thermo-mechanical simulator GLEEBLE 3800. A *K*-type thermocouple was welded onto the midsection of each coupon to control temperature during Q&P treatment. The accuracy of temperature control was ±1 °C.

A schematic drawing of the Q&P treatment is presented in Fig. 1. The samples were fully austenitized at 1100 °C for 15 min and quenched to the given quenching temperature with a cooling rate >1 °C/s and soaked at the quenching temperature for 20 s. It should be noted that only OQT of 160 °C was used for the alloy 410, whereas the remaining two alloys were quenched to OQT or room temperature (RTQ), which was in the range of 28–30 °C. The quenching step was followed by heating with the heating rate of 10 °C/s to partitioning temperature (PT), partitioning for the given time (Pt), and quenching to room temperature with the cooling rate of >1 °C/s. All three steels were partitioned at 450 °C for 5 min (see Section 2.2). Additionally, to study the effect of PT and Pt on the microstructure and properties, alloy 410 was partitioned at 400 °C for 5 min or at 450 °C for 2 min. At least three coupons were Q&P treated for each condition. Hereafter, all Q&P processed samples will be designated as 'alloy-QT-PT-Pt'.

2.4. Microstructural characterization

Quantitative microstructural characterization of the Q&P treated samples was performed through electron backscatter diffraction (EBSD) analysis. Specimens were ground and polished to a mirror-like surface applying standard metallographic techniques with final polishing using colloidal silica suspension (OPS). The EBSD studies were performed using an FEI Quanta™ Helios NanoLab 600i equipped with a Nordlys-Nano detector controlled by the AZtec Oxford Instruments Nanoanalysis (version 2.4) software. The data were acquired at an accelerating voltage of 20 kV, a working distance of 8 mm, a tilt angle of 70°, and a step size of 100 nm. The orientation data were post-processed using HKL Post-processing Oxford Instruments Nanotechnology (version 5.1©) software and TSL Data analysis version 7.3 software. Grain boundaries having a misorientation of ≥15° were defined as high-angle grain boundaries (HAGBs), whereas low-angle grain boundaries (LAGBs) had a misorientation of <15°. The volume fractions of tempered martensite, fresh martensite and retained austenite present in each EBSD micrograph were determined by a two-step procedure [23]. In this procedure, retained austenite and martensite are separated in the first step (Fig. 5a). In the second step, fresh martensite (FM) and tempered martensite (TM) are separated using the grain average image quality (GAIQ) criterion (Fig. 5b). Grain size was calculated as an average grain diameter. The prior austenite grain size was measured by reconstructing the austenite grains using the MTEX package for Matlab, and specifically, a routine developed by T. Nyyssönen [24]. The microstructure was observed on the plane perpendicular to the sample transverse direction (the RD–ND plane).

Additional XRD studies were performed to measure the volume fraction of retained austenite and carbon content therein. The XRD measurements were carried out on a diffractometer (Empyrean, PANalytical) with Cu K_α radiation ($\lambda = 0.1506$ nm) at 45 kV and 40 mA. The scans were performed in the range of 40–105° with a step size of 0.05°. The lattice parameter of the austenite was calculated using the peak positions of the four austenite peaks and the Nelson-Riley function; the latter was used to correct the sample displacement. Carbon content was calculated following the methodology described in Ref. [25].

To study nanoscale carbides formed in the 420ma alloy, transmission electron microscopy (TEM) studies were carried out using a FEG S/TEM (Talos F200X, FEI) operated at an accelerating voltage of 200 kV. Thin foils were prepared on a TenuPol 5 (Struers®) by twin-jet electropolishing with 10% perchloric acid in acetic acid at 15 °C at an operating voltage of 40 V. TEM imaging was carried out in bright-field (BF) and

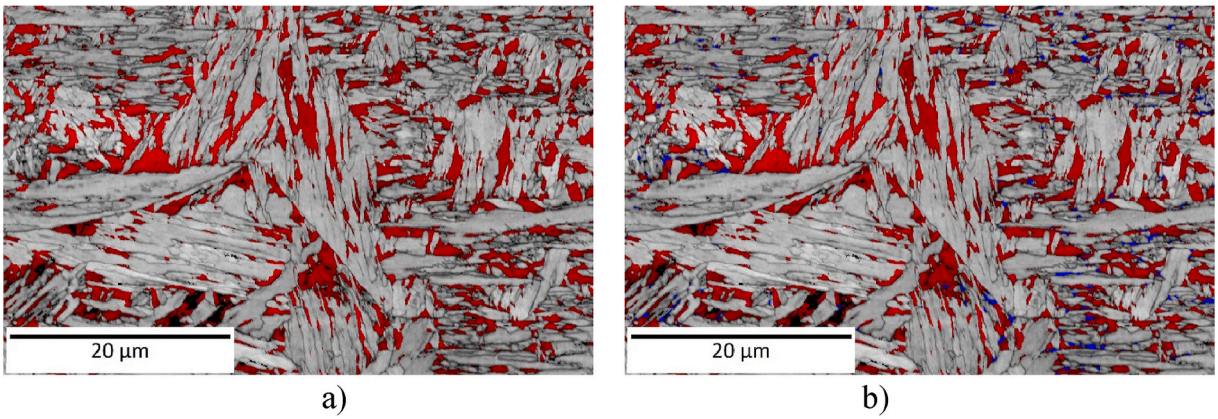

Fig. 5. A typical EBSD phase map of 420ma-OQT-450-5 sample with identified microstructural constituents: a) in the first step, retained austenite (RA) in the martensitic matrix is detected; b) in the second step, fresh martensite (FM) and tempered martensite (TM) are discriminated. FM is in blue, RA is in red, and TM is the matrix. (For interpretation of the references to colour in this figure legend, the reader is referred to the Web version of this article.)

high-angle annular dark field (HAADF) modes. Elemental mapping was carried out using energy dispersive spectroscopy (EDS) detector SuperX (4 detectors) from FEI & Bruker, integrated in the TEM.

2.5. Tensile testing

Sub-size tensile samples with a gauge length of 4 mm and a gauge width of 1 mm were machined from the midsection of the Q&P treated coupons. The tensile axis was parallel to the rolling direction. The surface of the machined samples was carefully ground to remove the oxide layer, so the final thickness of the samples was ~0.9 mm. Tensile tests were carried out at room temperature and initial strain rate of 10^{-3} s^{-1} using a Kammrath&Weiss testing module. The outcomes of tensile tests were analyzed, and basic mechanical properties (yield strength $\sigma_{0.2}$, ultimate tensile strength σ_{UTS}, uniform elongation ε_u, and total elongation ε_t) were measured. In order to estimate the strain hardening exponent n, true stress – true strain curves were plotted and fitted by the simple power law $\sigma = K\varepsilon^n$, where K is the strength coefficient. At least two tests were performed for each condition, and the results were found to be reproducible.

3. Results

3.1. Microstructure of the Q&P treated steels

Fig. 6 illustrates typical EBSD band contrast maps overlaid by an inverse pole figure (IPF) map for retained austenite grains and corresponding kernel average misorientation (KAM) maps. The alloys/conditions showing the highest (Fig. 6c), average (Fig. 6a) and lowest (Fig. 6b) local volume fractions of retained austenite are presented. The retained austenite grains are homogeneously distributed over the microstructure of all studied samples. Two morphologies of retained austenite can be noted: blocky morphology (relatively large equiaxed grains having a size of ≥1 μm) and interlath morphology (finer elongated grains). Retained austenite grains do not show any preferred crystallographic orientation (Fig. 6). The lath structure of the martensitic matrix is also clearly seen. The KAM maps (Fig. 6) demonstrate that the interior of martensite lath has nearly zero misorientation, whereas the martensite lath boundaries show higher misorientation of 1 ….1.5°. Some ultra-fine non-indexed areas on the maps (white pixels on the KAM maps, Fig. 6) may correspond to fresh martensite, which could not be indexed, as the high carbon content results in high lattice distortion [23,26]. They are usually adjacent to retained austenite grains. Also, the grain, packet, block and lath boundaries cannot be indexed due to overlapping patterns.

The local volume fractions of the microstructural constituents and their size after different Q&P treatments applied to the studied alloys are listed in Table 2 and Table 3, respectively. The histograms of grain size distribution for retained austenite are compared in Fig. 7. It is seen that the increase of the partitioning temperature and time is beneficial for the 410 alloy, as the local volume fraction of retained austenite increases from 6.7% to 9.6% (Table 2). There is no significant effect of the Q&P parameters on the retained austenite grain size. As is well known, lath martensite is characterized by a hierarchical sub-grain structures comprising packets, blocks and laths of particular crystallography [27]. These microstructural constituents of the martensitic matrix in all studied alloys vary widely in size and do not show a clear dependence on the applied Q&P treatment parameters (Table 3).

There is a dramatic effect of quenching temperature on the microstructure of the 420 alloy. The local volume fraction of retained austenite measured by EBSD drops significantly from 9.7% to 0.4% with decreasing quenching temperature (Fig. 6b, Table 3), and the formation of retained austenite grains with a size above 1 μm is fully suppressed (Figs. 6b and 7b). The increase of Mn content and additional microalloying by Nb and Ti (alloy 420ma, Table 1) benefits the volume fraction of retained austenite, which increases to 14.5–15.5% (Table 2). This is related to the additional stabilization of retained austenite by Mn [10]. Also, microalloying by Nb and Ti results in the formation of nanoscale NbC and TiC particles in the alloy 420ma (Fig. 8). They are typically formed during hot rolling of such steels and characterized by very high thermal stability [28,29]. They have a spherical shape with the average size of 81 ± 26 nm and 43 ± 16 nm, respectively (Fig. 8). The NbC precipitates tend to decorate TiC nanoprecipitates. According to the thermodynamic analysis carried out in the earlier works, the formation of such complex precipitates is the result of the precipitation sequence of particles, TiC followed by NbC, where a newly formed NbC particle precipitates on the habit plane of a pre-existing TiC particle [30]. The habit plane is the interface with the lowest misfit between the secondary NbC particle and the pre-existing TiC particle. The Q&P treatment parameters do not affect the morphology and size of NbC and TiC nanoparticles.

It has been well known that both NbC and TiC nanocarbides effectively pin grain boundaries thus refining the microstructure during thermo-mechanical processing [28,29]. Indeed, the prior austenite grains in the 420ma alloy are smaller (21.7 μm) compared to those in the 410 and 420 alloys (37.7 μm and 36.2 μm, respectively) (Table 3). The finer prior austenite grain size in the 420ma alloy results in the finer martensite packet size (Table 3) [31]. It should be noted that the finer prior austenite grains could be an additional factor leading to the enhanced volume fraction of retained austenite in the Q&P treated 420ma alloy. In Ref. [18], Celada-Casero et al. demonstrated that provided the sufficient volume fraction of primary martensite, and that the

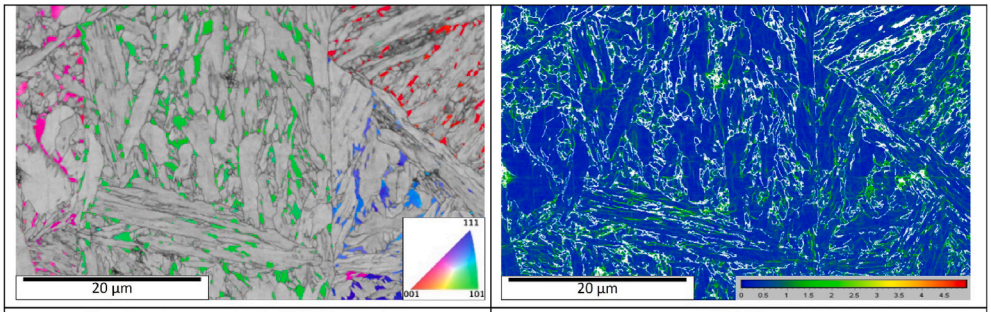

Retained austenite in IPF Z overlay | KAM

410-OQT-450-5 (Average local volume fraction of retained austenite, 9.6 %)

a)

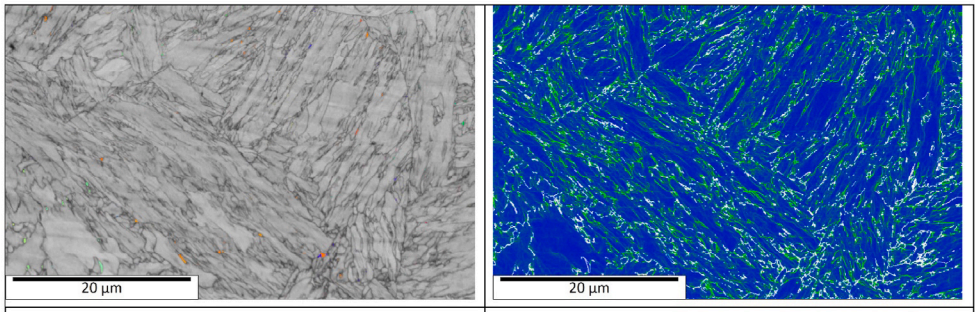

Retained austenite in IPF Z overlay | KAM

420-RTQ-450-5 (Lowest local volume fraction of retained austenite, 0.4 %)

b)

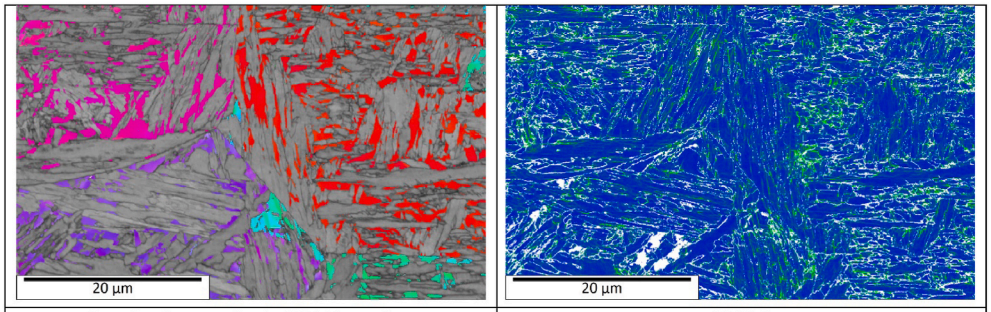

Retained austenite in IPF Z overlay | KAM

420ma-OQT-450-5 (Highest local volume fraction of retained austenite, 15.5 %)

c)

Fig. 6. Typical microstructures of the Q&P treated samples: a) 410-OQT-450-5 (with the average local volume fraction of retained austenite); b) 420-RTQ-450-5 (with the lowest local volume fraction of retained austenite); c) 420ma-OQT-450-5 (with the highest local volume fraction of retained austenite). Left: EBSD band contrast map overlaid by retained austenite IPF map; Right: KAM map of the corresponding area. (For interpretation of the references to colour in this figure legend, the reader is referred to the Web version of this article.)

partitioning conditions ensure the partitioning of all carbon to the surrounding austenite, finer prior austenite grain sizes result in a faster and more efficient carbon partitioning process than coarser microstructures through the formation of smaller and more homogeneously distributed phases during the first quench. Similar effect of finer prior austenite grain size on the volume fraction of retained austenite was also recently reported in another work [26].

The XRD technique provided higher fractions of retained austenite for all studied alloys compared to the EBSD method (Table 4). There are two main reasons for this observation. First, the interlath retained austenite grains having thickness well below the step size used in the EBSD measurements (100 nm) [32] and film-type retained austenite having a thickness less than 50 nm [33] cannot be detected by EBSD analysis. Second, using the XRD technique we measure the volume fraction of retained austenite on a larger area of ~1 mm^2, and it also includes the sub-surface volume. Meanwhile, EBSD measurements are limited to a surface area having a size of ~50 μm × 30 μm (Fig. 6). It should be noted that the fractions of finest interlath retained austenite and film-like retained austenite can vary in different alloys, thus resulting in varying difference between volume fractions of retained austenite measured by XRD and EBSD. Nevertheless, there is a good correlation between the outcomes of the EBSD and XRD analyses (Table 4). In the 410 alloy, the carbon content in retained austenite tends to increase from 0.85 wt % to 0.98 wt % with the increasing partitioning temperature and time due to the higher amount of carbon atoms diffused into retained austenite [18]. Also, a significant drop of austenite content in the 420 alloy with the decreasing quenching temperature leads to a noticeable increase of carbon content therein. In the 420-RTQ-450-5 sample, a very high fraction of primary martensite (i.e. a very low fraction of retained austenite) provides a significant amount of carbon to the austenite, thus resulting in the increased carbon content [18].

3.2. Tensile behaviour

Fig. 9 presents engineering stress – engineering strain curves from tensile testing of the Q&P treated alloys. The basic tensile mechanical properties and strain hardening exponent *n* were determined from the curves and summarized in Table 5. The following observations can be noted.

Table 2
Local volume fractions of the individual microstructural constituents measured by EBSD.

Alloy	Sample	Local volume fractions of microstructural constituents [%]			Non-indexed pixels [%]
		Retained austenite	Tempered martensite	Fresh martensite	
410	410-OQT-400-5	6.7	74.7	2.6	16.0
	410-OQT-450-2	6.7	77.3	5.3	10.7
	410-OQT-450-5	9.6	74.8	3.3	12.3
420	420-OQT-450-5	9.7	75.6	2.3	12.4
	420-RTQ-450-5	0.4	86.3	5.7	7.6
420ma	420ma-OQT-450-5	15.5	61.1	4.4	19
	420ma-RTQ-450-5	14.5	67.3	3.6	14.6

All Q&P treated alloys show ultimate tensile strength (UTS) above 1300 MPa and total elongation above 19%. In alloy 410, the yield strength (YS), uniform elongation and total elongation tend to increase with the increasing partitioning temperature and time, whereas ultimate tensile strength and strain hardening exponent show an opposite trend. The QP treated alloy 420 shows better mechanical strength compared to the 410 alloy. There is no significant effect of quenching temperature on the strength properties of the 420 alloy, whereas its total elongation and average *n*-values decrease, and uniform elongation dramatically drops with the decreasing quenching temperature. Despite significant strain hardening at the early stage of plastic deformation of the 420-RQT-450-5 (Fig. 9), the necking onsets at the plastic strain of 7.2%. The micro-alloyed alloy 420ma shows intermediate UTS values (1524 MPa) compared to the other two alloys, combined with sufficient uniform elongation values (15.2–17.1%). There is not significant effect of quenching temperature on strength of the 420ma alloy, whereas its total elongation decreases with the increasing quenching temperature (RTQ vs. OQT).

Data on mechanical properties of conventional quenched and tempered martensitic stainless steels have also been added in Table 5 for comparison. It is seen that the Q&P processed 410 alloy shows much better strength and ductility compared to the conventional quenched and tempered 410 alloy. Meanwhile, both Q&P treated 420 and 420ma alloys demonstrate similar level of strength as the conventional counterpart quenched and tempered at low temperatures.

4. Discussion

The outcomes of the microstructural characterization (Section 3.1) and tensile testing (Section 3.2) clearly show a strong effect of the Q&P treated microstructure on the tensile mechanical properties. Mechanical behavior of martensitic stainless steels containing retained austenite is determined by the interplay of several factors which are considered below.

4.1. The role of retained austenite

It is well known, that the volume fraction, size and stability of retained austenite grains play the key role in the mechanical behavior of AHSS [5–8,10]. A positive effect of the enhanced volume fraction of retained austenite (Table 2) on the uniform elongation values (Table 5) can be noted for all studied Q&P treated alloys. For example, the uniform elongation of the alloy 420 increases from 7.2% to 18.1% with the increasing local volume fraction of retained austenite from 0.4% to 9.7% (Table 2, Table 5). Earlier in situ studies of strain partitioning between phases in carbon steels showed that blocky retained austenite accommodates much higher local plastic strains compared to the martensitic matrix before its transformation [35,36]. Transformation of plastically deformed metastable blocky and interlath retained austenite grains under applied loading provides additional ductility due to the TRIP effect [5,10].

EBSD analysis of the Q&P treated samples after tensile testing of the five selected conditions revealed dramatic reduction of the volume fraction of retained austenite in all Q&P treated steels (Fig. 10, Table 6). Histograms of blocky and interlath retained austenite size distribution before and after tensile deformation of the selected conditions are compared in Fig. 11. It is seen that the austenite grains remaining after plastic deformation are much finer compared to those present in the microstructure before testing. Most blocky and larger interlath retained austenite grains transformed into martensite (Table 6). This is related to the higher stability of the fine interlath retained austenite grains [10]. Carbon content in retained austenite grains plays another important role. The higher is the carbon content, the higher is the stability of retained austenite [10]. From Table 4, it is seen that the increasing partitioning temperature and partitioning time in the alloy 410 leads to the higher carbon content in retained austenite [37], which, in turn, promotes its stability during plastic deformation [10]. Gradual transformation of retained austenite during tensile deformation maintains steady strain hardening, thus delaying the onset of necking [38,39].

It is known that metastable retained austenite grains with different crystallographic orientations have different stability during uniaxial tensile loading [10,40]. However, from the IPF maps, it is seen that the remaining retained austenite grains do not show any preferred crystallographic orientation (Fig. 10c). It can be suggested that the stress partitioning between martensite and austenite along with the constraining effect of the martensitic lath minimizes this effect. Indeed, a number of articles reported that crystallographic orientation plays a secondary role in affecting the austenite stability compared to its grain size [41] and chemical composition [42].

Table 3
Size of the individual microstructural constituents measured by EBSD.

Alloy	Condition	Microstructural parameters [μm]				
		Retained austenite grain size	Martensite packet size	Martensite block size	Martensite lath size	Prior austenite grain size
410	410-OQT-400-5	0.6 ± 0.2	17.5 ± 8.2	3.1 ± 1.3	0.9 ± 1.2	37.7 ± 9.7
	410-OQT-450-2	0.6 ± 0.2	12.3 ± 7.8	3.3 ± 1.9	0.6 ± 0.8	
	410-OQT-450-5	0.7 ± 0.3	11.3 ± 4.8	2.9 ± 0.7	0.7 ± 1.0	
420	420-OQT-450-5	0.7 ± 0.4	13.2 ± 2.0	2.4 ± 0.4	0.5 ± 0.9	36.2 ± 16.7
	420-RTQ-450-5	0.5 ± 0.1	16.2 ± 5.3	2.8 ± 0.9	0.9 ± 1.0	
420ma	420ma-OQT-450-5	0.8 ± 0.5	9.9 ± 5.1	2.8 ± 0.7	0.7 ± 0.9	21.7 ± 4.1
	420ma-RTQ-450-5	0.8 ± 0.5	11.0 ± 3.4	2.5 ± 0.8	0.7 ± 1.1	

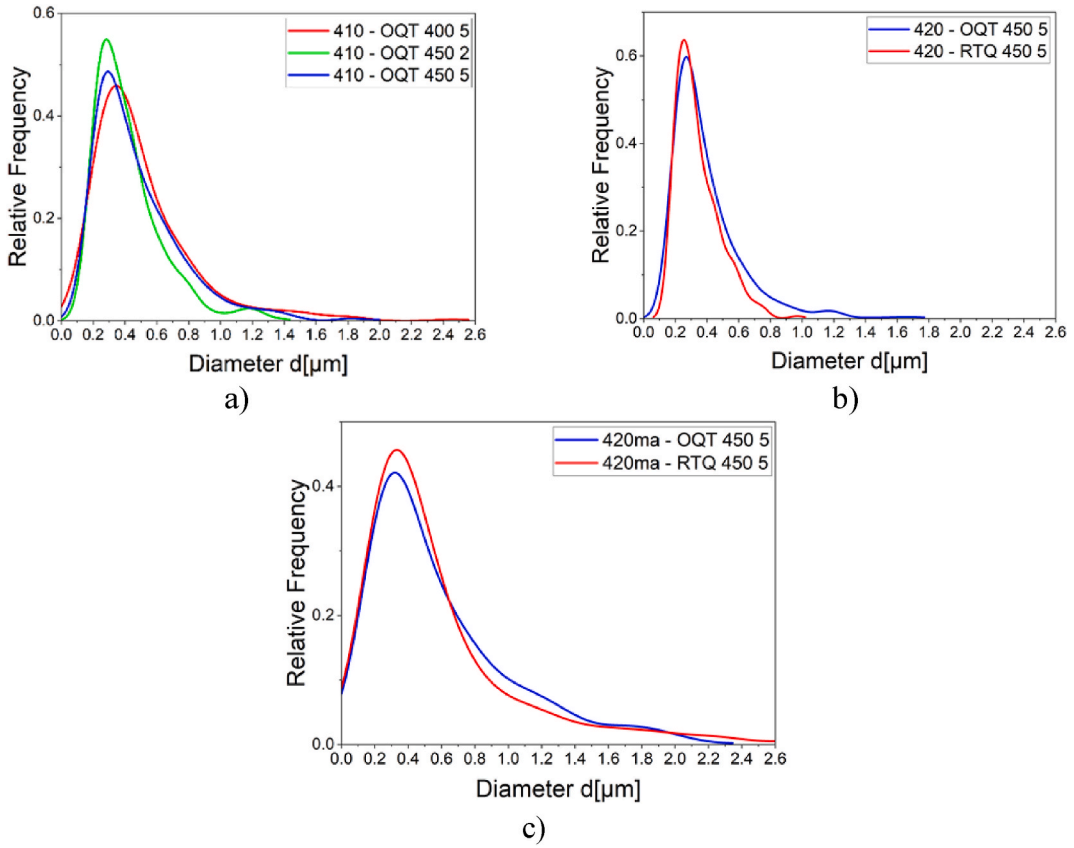

Fig. 7. Histograms of grain size distribution for retained austenite in the Q&P treated: a) alloy 410; b) alloy 420; c) alloy 420ma. (For interpretation of the references to colour in this figure legend, the reader is referred to the Web version of this article.)

Despite the 420ma alloy has the higher Mn content and is additionally microalloyed by Nb and Ti, its strength is surprisingly lower compared to the alloy 420 independently on the applied quenching temperature (Table 5). This observation can be rationalized based on the much higher volume fraction of blocky retained austenite in 420ma alloy compared to the 420 alloy (Table 6). The 420ma-RTQ-450-5 sample contains 10.3% of blocky retained austenite, whereas the latter is absent in the 420-RTQ-450-5 sample (Table 6). Plastic deformation begins with localized plastic flow in the soft blocky retained austenite grains, spreading to martensitic matrix due to dislocation hardening and/or austenite-martensite phase transformation at the later stage of plastic deformation [35,36]. An increasing fraction of the blocky retained austenite in the microstructure of the 420ma alloy leads to softening of the material and to the lower YS- and UTS-values. Meanwhile, the NbC and TiC nanocarbides do not provide significant strengthening effect (see Section 4.3).

4.2. The role of martensitic matrix

There is a significant body of experimental research showing the relationship between microstructural parameters of the martensite and mechanical properties. The martensite packet size plays the key role in controlling yield strength and ductile-brittle transition temperature (DBTT) [43]. The finer it is, the higher the yield strength and the lower the DBTT are. This effect, however, cannot be analyzed in our steels due to the minor variation in martensite packet size with Q&P parameters in the given alloy (Table 3).

Ability of the martensitic matrix to accumulate plastic deformation without its localization is an important factor determining ductility of the Q&P treated steels [26,44]. Qualitative analysis of the KAM maps before (Fig. 6) and after tensile deformation (Fig. 10) clearly shows increased misorientations in both the martensitic matrix and remaining retained austenite grains of the deformed material, which indicates high density of geometrically necessary dislocations (GNDs) accumulated in the microstructure [45]. Also, the higher fraction of fresh martensite in the deformed material further increases the fraction of the non-indexed pixels. Histograms of the local misorientation distribution in the Q&P treated steels before and after tensile deformation are compared in Fig. 12. It is clearly seen that plastic deformation shifts the histograms towards higher misorientation values. This shift is especially pronounced in the 420ma alloy (Fig. 12d and e) showing the highest uniform elongation values (Table 5). On the contrary, the lowest increase in misorientation values is demonstrated by the 420-RTQ-450-5 alloy (Fig. 12c) which has the lowest uniform elongation (Table 5).

4.3. About the role of the nanocarbides

It is well known that the interaction of nanocarbides with the gliding dislocations results in additional strengthening [29]. There are two well-known mechanisms of dislocation-particle interaction at room temperature: Orowan mechanism (or dislocation looping at the particle) and the cutting mechanism [46]. Their activation during plastic deformation strongly depends on the particle size. It was demonstrated that the critical particle diameter for the cutting mechanism is below 7–10 nm for the NbC and TiC carbides, whereas the Orowan mechanism can activate above that size [47]. The size of both NbC and TiC in the 420ma alloy are well above the threshold value (Fig. 8), so the Orowan mechanism is active in our case. The strengthening effect due to the Orowan mechanism can be estimated using the equation [48].

$$\Delta\sigma = k\frac{0.277Gb\sqrt{f}}{r}ln\left(\frac{r}{1.22b}\right) \quad (4)$$

where G is the shear modulus of the matrix, b the magnitude of the Burgers vector, f the volume fraction of particles, and r the particle

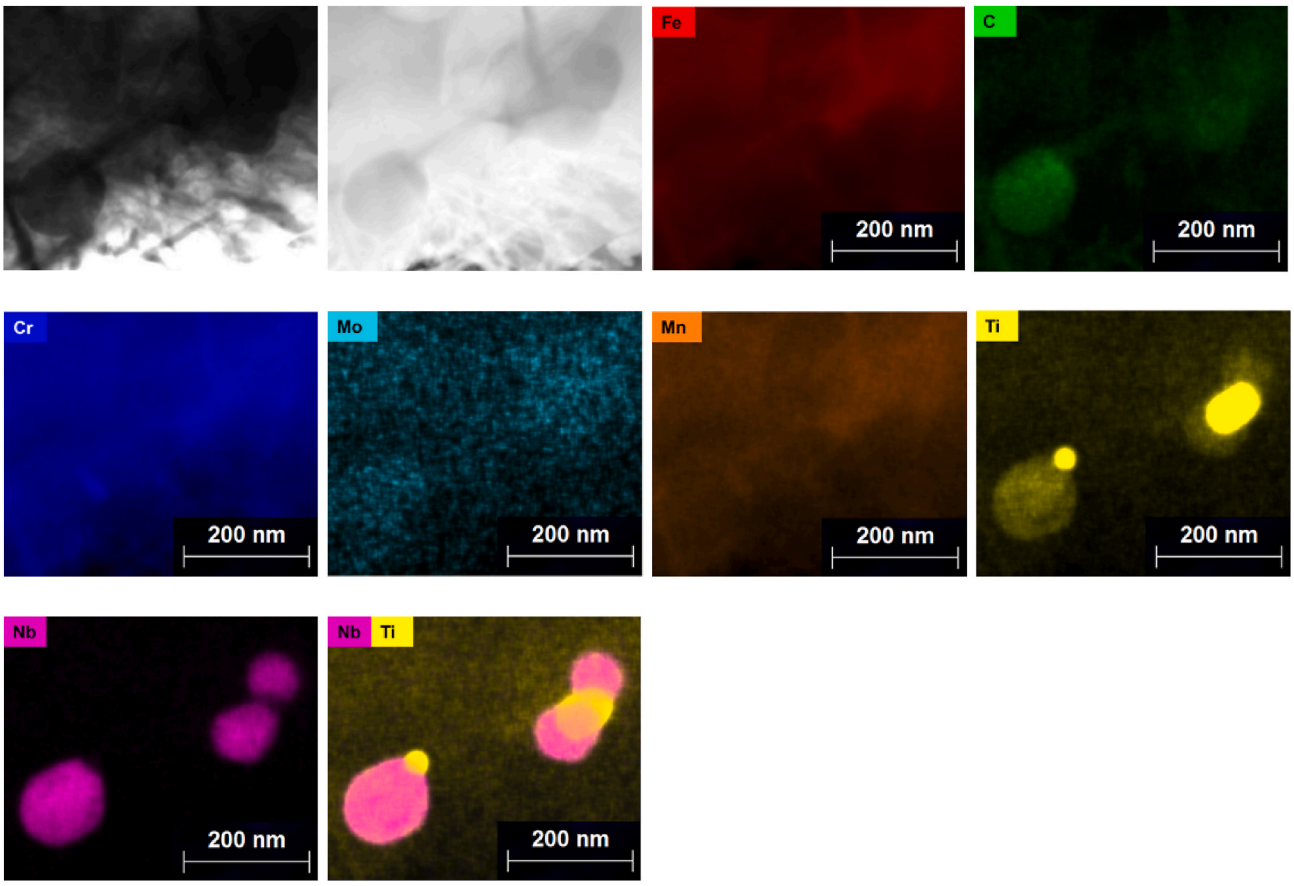

Fig. 8. BF and HAADF images with corresponding elemental maps of the sample 420ma-OQT-450-5.

Table 4
Volume fraction of retained austenite and carbon content measured by XRD and comparison with the EBSD data.

Alloy	Sample	Volume fractions of retained austenite [%]		Lattice parameter [Å]	Carbon content [wt. %]
		EBSD	XRD		
410	410-OQT-400-5	6.7	15.6	3.595	0.85
	410-OQT-450-2	6.7	14.6	3.598	0.91
	410-OQT-450-5	9.6	17.1	3.601	0.98
420	420-OQT-450-5	9.7	11.3	3.601	0.98
	420-RTQ-450-5	0.4	1.0	3.608	1.14
420ma	420ma-OQT-450-5	15.5	19.0	3.598	0.85
	420ma-RTQ-450-5	14.5	19.5	3.596	0.83

radius. TEM analysis does not allow to precisely estimate the volume fraction of nanocarbides in the material, as it is a very local tool. The EDX analysis in TEM did not reveal any presence of Nb or Ti elements in the matrix. Therefore, it can be suggested that all Nb and Ti atoms were effectively used for the formation of carbides. So, we can estimate the volume fraction of NbC and TiC: 0.055% and 0.098%, respectively.

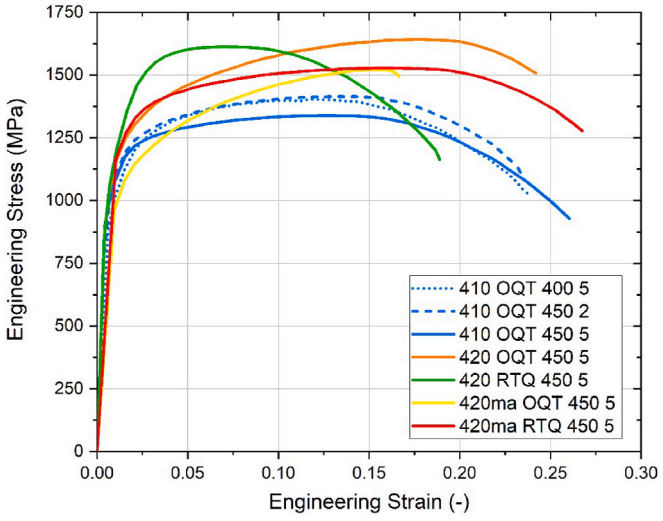

Fig. 9. Typical engineering stress – engineering strain curves for the Q&P treated alloys. (For interpretation of the references to colour in this figure legend, the reader is referred to the Web version of this article.)

Introducing all the data[1] into Eq. (4), we obtain that the precipitation hardening from NbC and TiC does not exceed 19 MPa and 41 MPa, respectively. Provided that most of the TiC are decorated by NbC, their joint strengthening effect should be even lower. Therefore, it can be

[1] G = 80.3 GPa, b = 0.248 nm, k = 1.21 [41].

Table 5
Basic tensile mechanical properties of the Q&P treated martensitic stainless steels and their conventional quenched and tempered counterparts.

Alloy	Condition	YS [MPa]	UTS [MPa]	ε_u [%]	ε_t [%]	n	Ref.
410	410-OQT-400-5	880	1403	11	23.3	0.13	This work
	410-OQT-450-2	950	1388	12.5	25.6	0.11	
	410-OQT-450-5	1007	1335	16.5	28.4	0.10	
420	420-OQT-450-5	1120	1655	18.1	24.2	0.15	
	420-RTQ-450-5	1152	1605	7.2	19.4	0.12	
420ma	420ma-OQT-450-5	943	1524	17.1	19.3	0.18	
	420ma-RTQ-450-5	1059	1524	15.2	26.5	0.12	
AISI 410	Quenched and tempered at relatively low temperature	620	830	–	12	–	ASTM standard [34]
AISI 410	Quenched and tempered at relatively high temperature	550	690	–	12	–	
AISI 420	Quenched and tempered at relatively low temperature	1360	1600	–	12	–	
AISI 420	Quenched and tempered at relatively high temperature	810	1035	–	18	–	

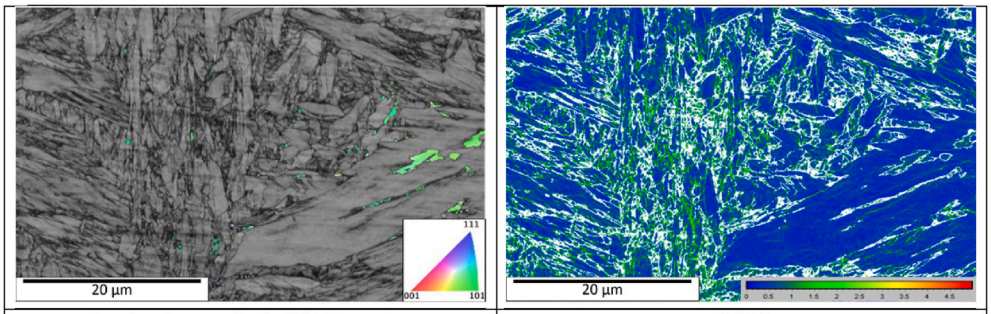

Retained austenite in IPF Z overlay | KAM

410-OQT-450-5 (Average local volume fraction of retained austenite, 9.6 % – After tensile test, 0.8 %)

a)

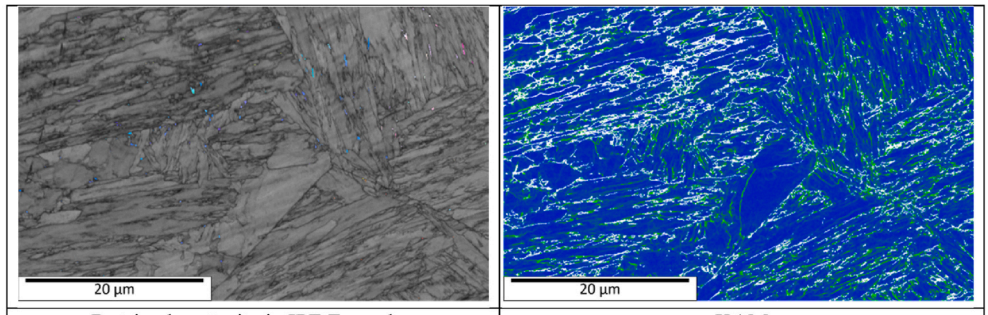

Retained austenite in IPF Z overlay | KAM

420-RTQ-450-5 (Lowest local volume fraction of retained austenite, 0.4 %) – After tensile test, 0.2 %)

b)

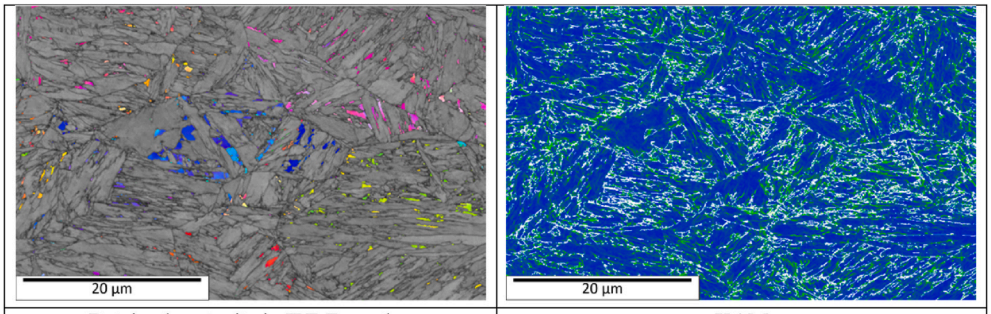

Retained austenite in IPF Z overlay | KAM

420ma-OQT-450-5 (Highest local volume fraction of retained austenite, 15.5 % – After tensile test, 2.9 %)

c)

Fig. 10. Typical microstructure of the Q&P treated samples after tensile testing: a) 410-OQT-450-5 (with initial average local volume fraction of retained austenite); b) 420-RTQ-450-5 (with initial lowest local volume fraction of retained austenite); c) 420ma-OQT-450-5 (with initial highest local volume fraction of retained austenite). Left: EBSD band contrast map overlaid by retained austenite IPF map; Right: KAM map of the corresponding area. (For interpretation of the references to colour in this figure legend, the reader is referred to the Web version of this article.)

concluded that both nanocarbides do not provide any significant additional hardening, and their primary role is the microstructure refinement.

4.4. About feasibility of the QP process in manufacturing martensitic stainless steels

Typically, martensitic stainless steels are manufactured by austenitising, quenching and tempering for at least 1 h [49]. For stainless steel

Table 6
Volume fraction (f^{γ}_{total}) and grain size (d^{γ}_{total}) of retained austenite before and after tensile deformation of the selected conditions. Data on volume fraction and grain size of blocky retained austenite (f^{γ}_{blocky} and d^{γ}_{blocky}, respectively) and interlath retained austenite (f^{γ}_{il} *and* d^{γ}_{il}, respectively) are also provided.

Sample	Before testing						After testing					
	Volume fraction of retained austenite			Grain size of retained austenite			Volume fraction of retained austenite			Grain size of retained austenite		
	f^{γ}_{total} [%]	f^{γ}_{blocky} [%]	f^{γ}_{il} [%]	d^{γ}_{total} [μm]	d^{γ}_{blocky} [μm]	d^{γ}_{il} [μm]	f^{γ}_{total} [%]	f^{γ}_{blocky} [%]	f^{γ}_{il} [%]	d^{γ}_{total} [μm]	d^{γ}_{blocky} [μm]	d^{γ}_{il} [μm]
410-OQT-450-5	9.6	3.0	6.6	0.7 ± 0.3	1.3 ± 0.2	0.4 ± 0.2	0.8	0.5	0.3	0.4 ± 0.3	1.6 ± 0.7	0.3 ± 0.2
420-OQT-450-5	9.7	2.5	7.2	0.7 ± 0.4	1.3 ± 0.1	0.4 ± 0.2	3.8	0.6	3.2	0.4 ± 0.2	1.3 ± 0.1	0.4 ± 0.2
420-RTQ-450-5	0.4	0	0.4	0.5 ± 0.1	0	0.5 ± 0.1	0.2	0	0.2	0.3 ± 0.1	0	0.3 ± 0.1
420ma-OQT-450-5	15.5	10.8	4.7	0.8 ± 0.5	1.5 ± 0.6	0.4 ± 0.2	2.9	0.6	2.3	0.4 ± 0.2	1.2 ± 0.2	0.3 ± 0.2
420ma-RTQ-450-5	14.5	10.3	4.2	0.8 ± 0.5	1.6 ± 0.6	0.4 ± 0.2	1.5	0.1	1.4	0.4 ± 0.2	1.3	0.4 ± 0.2

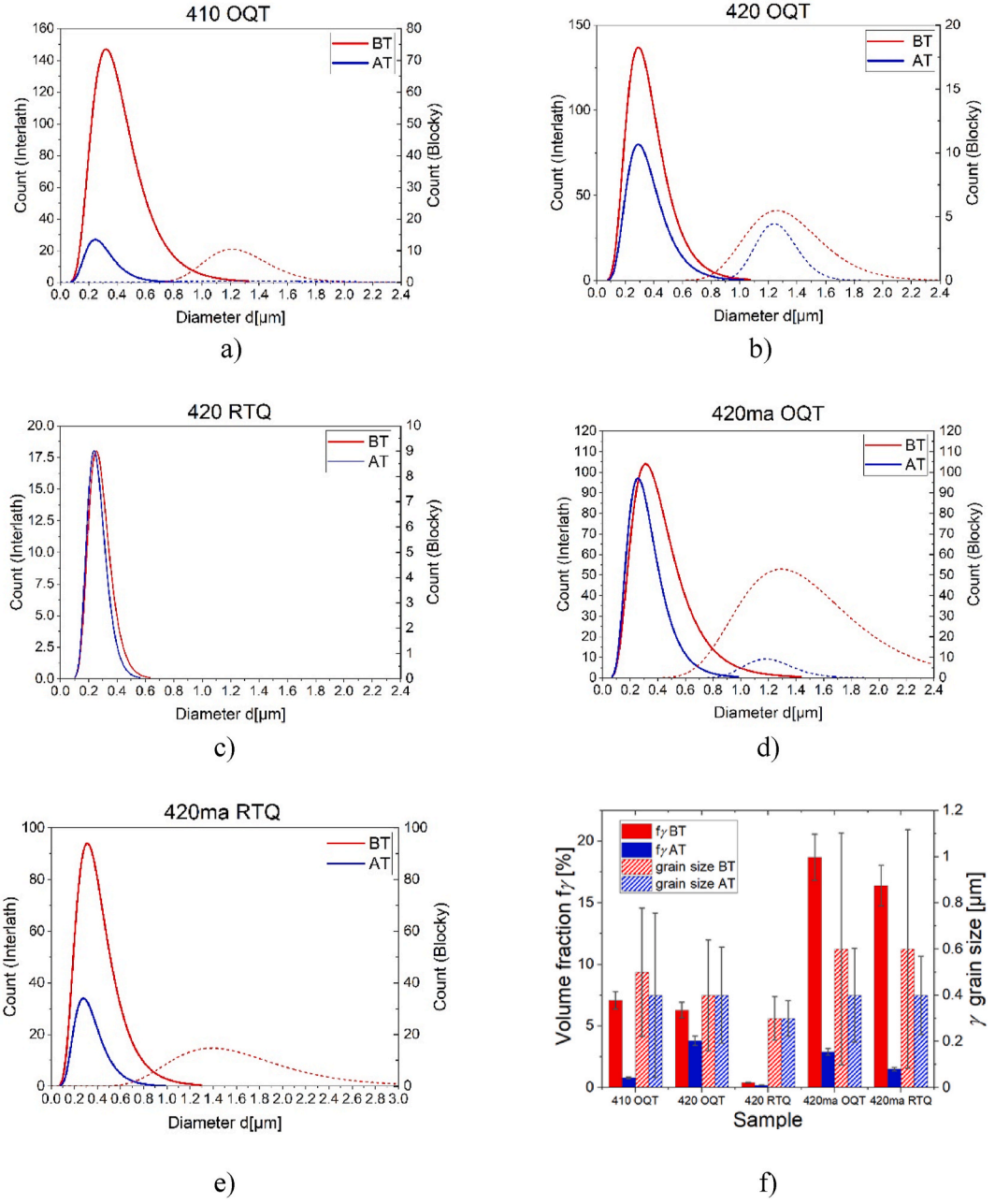

Fig. 11. (a–e) Histograms of the size distribution of blocky retained austenite (dashed lines) and interlath retained austenite (solid lines) before testing (BT) and after testing (AT) of: a) 410-OQT-450-5 alloy, b) 420-OQT-450-5 alloy, c) 420-RTQ-450-5 alloy, d) 420ma-OQT-450-5 alloy, e) 420ma-RTQ-450-5 alloy; f) a comparison of total volume fraction (f_{γ}) and grain size of retained austenite before testing (BT) and after testing (AT) in all studied samples. (For interpretation of the references to colour in this figure legend, the reader is referred to the Web version of this article.)

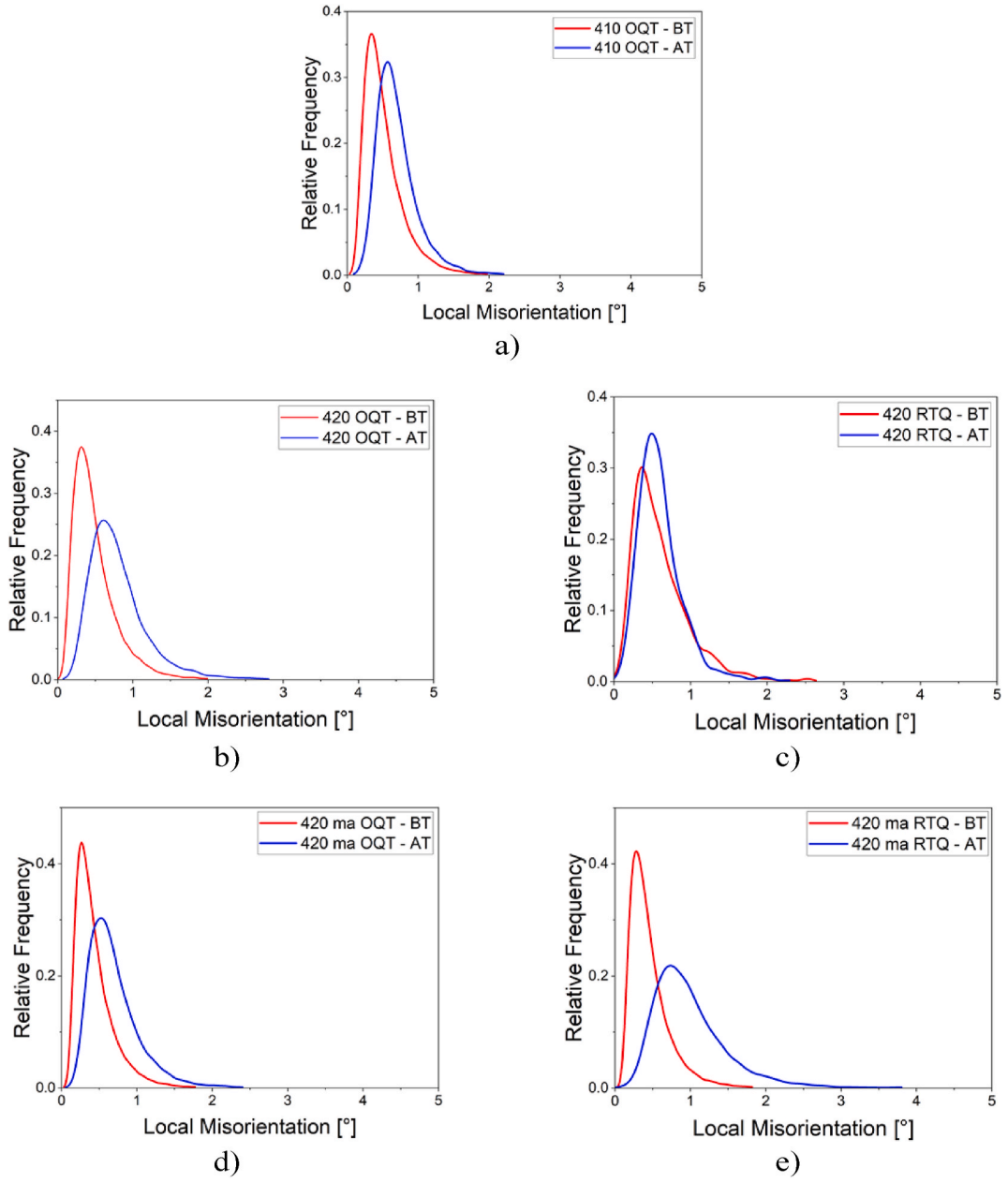

Fig. 12. Histograms of the local misorientation distribution before testing (BT) and after testing (AT) of: a) 410-OQT-450-5 alloy; b) 420-OQT-450-5 alloy; c) 420-RTQ-450-5 alloy; d) 420ma-OQT-450-5 alloy; e) 420ma-RTQ-450-5 alloy. (For interpretation of the references to colour in this figure legend, the reader is referred to the Web version of this article.)

industry, the benefits of the Q&P process are manyfold. First, its application would reduce the heat treatment time and, therefore, the energy consumption related with the manufacturing process. Unlike carbon steels, stainless steels with appropriate chemistry can be subjected to Q&P processing via quenching to room temperature (see Section 2.2). This provides additional advantages for the Q&P process from an industrial viewpoint, as there would be no need to control the quenching temperature on the industrial processing lines. The results presented in this work and earlier studies by other researchers [11,12] have demonstrated that a good combination of mechanical strength and ductility can be reached in martensitic stainless steels via Q&P processing. Improved fracture performance can be expected in the developed materials, as retained austenite improves fracture initiation toughness and crack growth resistance due to the TRIP-effect delaying crack propagation [50]. Also, carbon partitioned from martensite into austenite is expected to reduce the risk of interphase galvanic corrosion [51]. A deep understanding of the chemistry-process-microstructure-property relationship in these materials will enable a further tailoring their mechanical and application related properties for the benefit of end-users. Last but not least, application of the Q&P process allows to reduce the alloying cost by reducing Ni content by an order of magnitude. Currently, the vast majority of stainless steels contain between 8 and 11% of Ni. It is a very expensive metal which is also fast becoming one of the world's most critical elements [52].

5. Conclusions

The effect of alloying and Q&P treatment parameters on the microstructure and properties of martensitic stainless steels was experimentally studied. The following conclusions can be drawn based on the outcomes of this work.

Alloy chemistry and Q&P parameters (quenching temperature, partitioning temperature and partitioning time) significantly affect the

microstructure of the Q&P treated martensitic stainless steels. The volume fraction of retained austenite tends to increase with increasing partitioning temperature (from 400 °C to 450 °C) and partitioning time (from 2 min to 5 min). The highest volume fraction of retained austenite (15.5%) is reached in the chemistry with enhanced Mn content (3 wt%) and microalloyed by Ti and Nb (0.05 wt%). The martensitic packet size and lath size are not dependent on the considered parameters.

The Q&P treated martensitic stainless steels show a good combination of enhanced strength (UTS >1300 MPa) and sufficient tensile ductility (ε_t > 19%). Optimum Q&P parameters lead even to better combinations, such as UTS = 1655 MPa and ε_t = 24.2% (420-OQT-450-5 sample). In all studied alloys, the uniform elongation increases with the increasing volume fraction of retained austenite due to the TRIP effect. Most coarser blocky retained austenite grains transform to martensite during plastic deformation, whereas fine interlath retained austenite grains tend to remain in the microstructure due to their higher stability. EBSD analysis did not reveal any important role of crystallographic orientation in transformation stability of retained austenite during uniaxial tensile loading. Significant increase of the local misorientation values in KAM maps of the deformed samples indicates high ability of tempered martensitic matrix to accumulate plastic deformation.

CRediT authorship contribution statement

A. Sierra-Soraluce: Conceptualization, Investigation, Formal analysis, Visualization, Writing – original draft. **G. Li:** Investigation, Formal analysis, Data curation, Visualization, Writing – review & editing. **M.J. Santofimia:** Conceptualization, Supervision, Methodology, Project administration, Writing – review & editing. **J.M. Molina-Aldareguia:** Supervision, Resources, Methodology, Writing – review & editing. **A. Smith:** Conceptualization, Supervision, Project administration, Funding acquisition, Resources, Writing – review & editing. **M. Muratori:** Resources, Methodology, Project administration, Writing – review & editing. **I. Sabirov:** Conceptualization, Methodology, Supervision, Writing – review & editing, Project administration.

Declaration of competing interest

The authors declare that they have no known competing financial interests or personal relationships that could have appeared to influence the work reported in this paper.

Data availability

Data will be made available on request.

Acknowledgements

The authors would like to thank Dr. Manuel Avella Romero for the assistance provided with the TEM characterization and Dr. Javier Garcia Molleja for the support with the XRD measurements. The authors would like to acknowledge financial support by the Research Fund for Coal and Steel (RFCS) of European Union via QPINOX project (Grant Agreement 847195). Andres Sierra-Soraluce (IMDEA Materials Institute) gratefully acknowledges the financial support by the Maria de Maeztu seal of excellence from the Spanish Ministry of Science and Innovation (CEX2018-000800-M).

References

[1] S. Vögele, M. Grajewski, K. Govorukha, D. Rübbelke, Challenges for the European steel industry: analysis, possible consequences and impacts on sustainable development, Appl. Energy 264 (2020), 114633.
[2] S. Dieck, M. Ecke, T. Halle, P. Rosemann, Improvement of the martensitic stainless steel X46Cr13 by Q&P heat treatment, IOP Conf. Ser. Mater. Sci. Eng. 882 (2020), 012006.
[3] X. Hu, Z. Feng, Advanced High Strength Steel – Basics and Applications in the Automotive Industry. Report, Oak Ridge National Laboratory, USA, April 2021.
[4] J.G. Speer, D. Matlock, B. De Cooman, J. Schroth, Carbon partitioning into austenite after martensite transformation, Acta Mater. 51 (2003) 2611–2622.
[5] W. Bleck, X. Guo, Y. Ma, The TRIP effect and its application in cold formable sheet steels, Steel Res. Int. 88 (2017), 1700218.
[6] J.G. Speer, D.K. Matlock, L. Wang, D.V. Edmonds, Quenched and partitioned steels, Compre. Mater. Proc. 1 (2014) 217–225.
[7] J.G. Speer, E. De Moor, A.J. Clarke, Critical assessment 7: quenching and partitioning, Mater. Sci. Technol. 31 (2015) 3–9.
[8] D.V. Edmonds, E. De Moor, D.K. Matlock, J.G. Speer, Quenching and partitioning steel, in: Encyclopedia of Iron, Steel, and Their Alloys, CRC Press, 2016.
[9] L. Wang, J.G. Speer, Quenching and partitioning steel heat treatment, Metall. Microstr. Anal. 2 (2013) 268–281.
[10] E. Pereloma, A. Gazder, I. Timokhina, Retained austenite: transformation-induced plasticity, in: first ed., in: G.E. Totten, C. Rafael (Eds.), Encyclopedia of Iron, Steel, and Their Alloys, CRC Press, 2016, pp. 3088–3103.
[11] T. Tsuchiyama, J. Tobata, T. Tao, N. Nakada, S. Takaki, Quenching and partitioning treatment of a low-carbon martensitic stainless steel, Mater. Sci. Eng. 532 (2012) 585–592.
[12] J. Tobata, K. Ngo-Huynh, N. Nakada, T. Tsuchiyama, S. Takaki, Role of Si in quenching and partitioning treatment of low-carbon martensitic stainless steel, ISIJ Int. 52 (2012) 1377–1382.
[13] S.Y. Lu, K. Yao, Y. Chen, M. Wang, N. Chen, X. Ge, Effect of quenching and partitioning of the microstructure evolution and electrochemical properties of a martensitic stainless steel, Corrosion Sci. 103 (2016) 95–104.
[14] J. Mola, B.C. De Cooman, Quenching and partitioning (Q&P) processing of martensitic stainless steels, Metall. Mater. Trans. 44A (2013) 946–966.
[15] Q. Huang, C. Schroeder, H. Biermann, O. Volkova, J. Mola, Influence of martensite fraction on tensile properties of quenched and partitioned (Q&P) martensitic stainless steels, Steel Res. Int. 87 (2016) 1082–1094.
[16] S. Dieck, P. Rosemann, A. Kromm, T. Halle, Reversed austenite for enhancing ductility of martensitic stainless steel, IOP Conf. Ser. Mater. Sci. Eng. 181 (2017), 012034, https://doi.org/10.1088/1757-899X/181/1/01203.
[17] C. Celada-Casero, F. Vercruysse, B. Linke, A. Smith, P. Kok, J. Sietsma, M. J. Santofimia, Analysis of work hardening mechanisms in Quenching and Partitioning steels combining experiments with a 3D micro-mechanical model, Mater. Sci. Eng. 846 (2022), 143301.
[18] C. Celada-Casero, C. Kwakernaak, J. Sietsma, M.J. Santofimia, The influence of the austenite grain size on the microstructural development during quenching and partitioning processing of a low-carbon steel, Mater. Des. 178 (2019), 10784.
[19] C. Kung, J. Rayment, An examination of the validity of existing empirical formulae for the calculation of Ms temperature, Metall. Trans. A 13 (1982) 328–331.
[20] J.G. Speer, D.V. Edmonds, F.C. Rizzo, D.K. Matlock, Partitioning of carbon from supersaturated plates of ferrite, with application to steel processing and fundamentals of the bainite transformation, Curr. Opin. Solid State Mater. Sci. 8 (2004) 219–237.
[21] M.J. Santofimia, J.G. Speer, A.J. Clarke, L. Zhao, J. Sietsma, Influence of interface mobility on the evolution of austenite–martensite grain assemblies during annealing, Acta Mater. 57 (2009) 4548–4557.
[22] A.J. Clarke, J.G. Speer, D.K. Matlock, F.C. Rizzo, D.V. Edmonds, M.J. Santofimia, Influence of carbon partitioning kinetics on final austenite fraction during quenching and partitioning, Scripta Mater. 61 (2009) 149–152.
[23] M.J. Santofimia, R. Petrov, L. Zhao, J. Sietsma, Microstructural analysis of martensite constituents in quenching and partitioning steels, Mater. Char. 92 (2014) 91–95.
[24] T. Nyyssönen, Parent austenite reconstruction GUI, Retrieved on [09/05/2022] from: https://github.com/nyyssont/parent_austenite_reconstruction, 2020.
[25] N.H. van Dijk, A.M. Butt, L. Zhao, J. Sietsma, S.E. Offerman, J.P. Wright, S. van der Zwaag, Thermal stability of retained austenite in TRIP steels studied by synchrotron X-ray diffraction during cooling, Acta Mater. 53 (2005) 5439–5447.
[26] P. Xia, F. Vercruysse, C. Celada-Casero, P. Verleysen, R.H. Petrov, I. Sabirov, J. M. Molina-Aldareguia, A. Smith, B. Linke, R. Thiessen, D. Frometa, S. Parareda, A. Lara, Effect of alloying and microstructure on formability of advanced high-strength steels processed via quenching and partitioning, Mater. Sci. Eng. 831 (2022) 142217.
[27] S. Morito, X. Huang, T. Furuhara, T. Maki, N. Hansen, The morphology and crystallography of lath martensite in alloy steels, Acta Mater. 54 (2006) 5323–5331.
[28] J. Xing, G. Zhu, B. Wu, H. Ding, H. Pan, Effect of Ti addition on the precipitation mechanism and precipitate size in Nb-microalloyed steels, Metals 12 (2022) 245.
[29] A.G. Kostryzhev, O.O. Marenych, C.R. Killmore, E.V. Pereloma, Strengthening mechanisms in thermomechanically processed Nb-Ti microalloyed steel, Metall. Mater. Trans. 46 (2015) 3470–3480.
[30] H. Zhang, H. Xiong, First-principles study of NbC heterogeneous nucleation on TiC vs. TiN in microalloy steel, Ironmak. Steelmak. 47 (2018) 77–83.
[31] S. Morito, H. Saito, T. Ogawa, T. Furuhara, T. Maki, Effect of austenite grain size on the morphology and crystallography of lath martensite in low carbon steels, ISIJ Int. 45 (2005) 91–94.
[32] P. Xia, F. Vercruysse, R. Petrov, I. Sabirov, M. Castillo-Rodríguez, P. Verleysen, High strain rate tensile behavior of a quenching and partitioning (Q&P) Fe-0.25C-1.5Si-3.0Mn steel, Mater. Sci. Eng. 745 (2019) 53–62.
[33] J. Hidalgo, K.O. Findley, M.J. Santofimia, Thermal and mechanical stability of retained austenite surrounded by martensite with different degrees of tempering, Mater. Sci. Eng. 690 (2017) 337–347.

[34] Standard Specification for Stainless Steel Bars and Shapes. ASTM Standard A276/A276M – 17.
[35] A. Kumar, A. Dutta, S.K. Makineni, M. Herbig, R.H. Petrov, J. Sietsma, In-situ observation of strain partitioning and damage development in continuously cooled carbide-free bainitic steels using micro digital image correlation, Mater. Sci. Eng. 757 (2019) 107–116.
[36] I. de Diego-Calderon, M.J. Santofimia, J.M. Molina-Aldareguia, M.A. Monclus, I. Sabirov, Deformation behavior of a high strength multiphase steel at macro- and micro-scales, Mater. Sci. Eng. 611 (2014) 201–211.
[37] M.J. Santofimia, L. Zhao, J. Sietsma, Overview of mechanisms involved during the quenching and partitioning process in steels, Metall. Mater. Trans. 42 (2011) 3620.
[38] A. Grajcar, A. Skowronek, K. Radwanski, Mechanical behavior and stability of dispersed retained austenite in thermomechanically rolled and isothermally-treated TRIP-aided multiphase steel, Mater. Sci. Eng. 830 (2022), 142300.
[39] C.B. Finfrock, M.M. Thrun, D. Bhattacharya, T.J. Ballard, A.J. Clarke, K.D. Clarke, Strain rate dependent ductility and strain hardening in Q&P steels, Metall. Mater. Trans. 52 (2021) 928–942.
[40] O. Muránsky, P. Šittner, J. Zrník, E.C. Oliver, In situ neutron diffraction investigation of the collaborative deformation–transformation mechanism in TRIP-assisted steels at room and elevated temperatures, Acta Mater. 56 (2008) 3367–3379.
[41] D. De Knijf, C. Föjer, L.A.I. Kestens, R. Petrov, Factors influencing the austenite stability during tensile testing of Quenching and Partitioning steel determined via in-situ Electron Backscatter Diffraction, Mater. Sci. Eng. 638 (2015) 219–227.
[42] R. Blondé, E. Jimenez-Melero, L. Zhao, J.P. Wright, E. Brück, S. van der Zwaag, N. H. van Dijk, High-energy X-ray diffraction study on the temperature-dependent mechanical stability of retained austenite in low-alloyed TRIP steels, Acta Mater. 60 (2012) 565–577.
[43] Y. Tomita, K. Okabayashi, Effect of microstructure on strength and toughness of heat-treated low alloy structural steels, Metall. Trans. A 17 (1986) 1203–1209.
[44] I. de Diego-Calderon, D. De Knijf, M.A. Monclús, J.M. Molina-Aldareguia, I. Sabirov, C. Föjer, R.H. Petrov, Global and local deformation behavior and mechanical properties of individual phases in a quenched and partitioned steel, Mater. Sci. Eng. 630 (2015) 27–35.
[45] M. Calcagnotto, D. Ponge, E. Demir, D. Raabe, Orientation gradients and geometrically necessary dislocations in ultrafine grained dual-phase steels studied by 2D and 3D EBSD, Mater. Sci. Eng. 527 (2010) 2738–2746.
[46] J.W. Martin, Precipitation Hardening, second ed., Butterworth-Heinemann, 2012.
[47] S. Takaki, Strengthening of steel by secondary particles, in: Fundamentals and Applications of Precipitation in Steels, Iron and Steel Institute of Japan, Tokyo, 2001, pp. 69–80.
[48] D. Raabe, B. Sun, A. Kwiatkowski Da Silva, B. Gault, H.W. Yen, K. Sedighiani, P. T. Sukumar, I.R. Souza Filho, S. Katnagallu, E. Jagle, P. Kürnsteiner, N. Kusampudi, L. Stephenson, M. Herbig, C.H. Liebscher, H. Springer, S. Zaefferer, V. Shah, S. L. Wong, C. Baron, M. Diehl, F. Roters, D. Ponge, Current challenges and opportunities in microstructure-related properties of advanced high strength steels, Metall. Mater. Trans. 51 (2020) 5517–5586.
[49] ASM Handbook, in: Heat Treating vol. 4, ASM International Handbook Committee, Materials Park, OH, USA, 1991.
[50] I. de Diego-Calderon, I. Sabirov, J.M. Molina-Aldareguia, C. Föjer, R. Thiessen, R. H. Petrov, Microstructural design in quenched and partitioned (Q&P) steels to improve their fracture properties, Mater. Sci. Eng. 657 (2016) 136–146.
[51] T. Mehner, R. Morgenstern, P. Frint, I. Scharf, M.F.X. Wagner, T. Lampke, Corrosion characteristics of a quenching and partitioning steel determined by electrochemical impedance spectroscopy, IOP Conf. Ser. Mater. Sci. Eng. 373 (2018), 012003.
[52] B.A. McNulty, S.M. Jowitt, Barriers to and uncertainties in understanding and quantifying critical mineral and element supply, iScience 24 (2021), 102809.